

Estimation of glacier mass balance on a basin scale: an approach based on satellite-derived snowlines and a temperature index model

S. A. Tawde^{1,*}, A. V. Kulkarni² and G. Bala^{1,2,3}

¹Centre for Atmospheric and Oceanic Sciences,

²Divecha Centre for Climate Change, and

³Interdisciplinary Centre for Water Research, Indian Institute of Science, Bengaluru 560 012, India

Mass balance is an important metric to assess the growth or decline of water stored in a glacier. The Accumulation Area Ratio (AAR) method where mass balance is proportional to AAR has been used to estimate glacier mass balance by several studies in the past. Since field estimates of AAR are not feasible on every glacier, it is usually estimated by identifying the snowline at the end of ablation season as a proxy of Equilibrium Line Altitude (ELA) on satellite images. However, locating ELA on satellite images is challenging due to temporal gaps, cloud cover and fresh snowfall on glaciers. Hence, the highest observed snowline has been traditionally used to estimate AAR, which usually leads to an underestimate of mass loss. To rectify this problem we propose a method to estimate the position of ELA by combining satellite images with *in situ* meteorological observations and a snowmelt model. The main advantage of this method is that it can be used to estimate the mass balance of individual glaciers and basins. Application of the method to eight glaciers in the Chandra basin, Western Himalaya is found to reduce the bias in mass balance estimates compared to the traditional AAR technique and the modelled estimates are in good agreement with the geodetic method. When applied to 12 selected glaciers in the Chandra basin, the modelled cumulative mass balance is -1.67 ± 0.72 Gt (-0.79 ± 0.34 m w.e. a⁻¹) during 1999/2000–2008/09. This method can also be used to estimate the future deviations in mass balance using climate change projections of temperature and precipitation.

Keywords: Accumulation area ratio, equilibrium line altitude, glacier mass balance, temperature index model, transient snowline.

GLACIATED area covers 40,800 sq. km in the Himalaya and Karakoram region¹. Melt water from glaciers and seasonal snow is one of the major resources of the Himalayan rivers for sustaining the hydrological and socio-economic activities of the downstream population^{2,3}.

However, the diverse topography and climate of the Himalaya affect the amount and seasonality of water released from the glaciers. The water availability can be affected due to current and future climate change^{4–11}. This can affect biodiversity and ecosystems of the region¹². Therefore, it is important to assess the future water security in this region so that sound climate change adaptation policies can be developed.

Inter-annual variation in glacier run-off is correlated with annual change in mass of the glacier^{13,14}. Annual cycles of mass balance control glacial flow as well as expansion/contraction of glacier length and area¹⁵. Negative mass balance for several consecutive years could lead to thinning and retreat of the snout of glaciers. This process eventually reduces glacier area. The change in glacier area enhances/reduces the contribution to glacier-derived stream flows. In the initial decades of glacier retreat more melt water would be released, followed by cessation of melt water^{13,16}. Therefore, mass balance is one of the most important metrics to assess future changes in freshwater resources from glacier storage.

In the Himalaya, glacier mass balance is presently estimated by several methods. Glaciological method (also known as field estimate) is one of the most commonly used methods, where mass balance is estimated using *in situ* field studies. However, due to mountainous terrain and logistic reasons, this method is limited to a few glaciers. Hence, mass balance for most of the glaciated terrains is not available from field estimates. In the Western Himalaya, field measurements are available only for ten glaciers out of which only two – Hamtah and Chhota Shigri glaciers – have continual field mass balance records since the last decade¹⁷. Therefore, other methods such as geodetic and area accumulation ratio (AAR) have been used to estimate basin-wide glacier mass balance. The geodetic method uses digital elevation models (DEM) of different years. The geodetic method can provide information about volumetric loss on a regional scale and has been used in the Himalaya where satellite-derived DEMs are available^{18–21}.

The AAR method relies on a linear regression between mass balance and AAR^{22,23}. Kulkarni²² found a good

*For correspondence. (e-mail: sayli@caos.iisc.ernet.in)

correlation between field mass balance and AAR measurements on Shaune Garang and Gor Garang glaciers in the Baspa basin, Western Himalaya and developed a regression between these two variables. The calculation of AAR requires a knowledge of Equilibrium Line Altitude (ELA), which can be derived in field by interpolating observed mass balance to the elevation of zero net mass balance²⁴. Field-estimated ELA is not feasible for every glacier in a basin because of difficulties associated with access to mountainous terrain. However, snowlines are easily identifiable on satellite images and the transient snowline (TSL) at the end of the glaciological year coincides with ELA on temperate glaciers^{15,25–27}. Therefore, many studies in different parts of the Himalaya have used satellite-derived ELA^{23,28–31} and the resultant AAR in the regression developed by Kulkarni *et al.*²³ for estimation of glacier mass balance.

However, identifying ELA on satellite images could be a challenge because of temporal gaps in data, cloud cover and fresh snowfall events on the glacier during summer months^{32,33}. Therefore in practice, the highest snowline in ablation season is used as a proxy for ELA. Hence, the mass balance estimates from the AAR method are likely to deviate from field observations which usually take place at the end of September. Therefore, to improve mass balance estimates of the AAR method, we require a method to locate the position of TSL at the end of ablation season. Huss *et al.*³⁴ have demonstrated a method to monitor TSL in ablation season using terrestrial photographs, temperature index (TI) models. In the present study, we propose an approach similar to that of Huss *et al.*³⁴, to identify snowline at the end of ablation season using satellite images; *in situ* meteorological data and TI model to improve the conventional AAR method. We demonstrate that this method improves the mass balance estimates for some selected individual glaciers in the Chandra basin, Western Himalaya. Further, we demonstrate that this method can be applied on the basin scale by extending the mass balance estimates to 12 selected glaciers in the same basin.

Study area and data

The Chandra Basin

The study area, Chandra basin, is situated in the Lahaul–Spiti valley, Western Himalaya, Himachal Pradesh, India (Figure 1). This basin receives precipitation predominantly from western disturbances in the post-monsoon and winter period (October–April) (Figure 2). The area of the basin is $\sim 2.44 \times 10^3$ sq. km, with an elevation range 2800–6600 m amsl (ref. 35). There are 201 glaciers constituting 29.54% of the total basin area, of which we have selected 12 for the present study (Table 1). Two of the 12 (Chhota Shigri and Hamtah) glaciers have extensive field

measurements. The basis for selection of the 12 glaciers is: easily identifiable on satellite images, different orientations, and located in different regions of the basin so that the entire basin is approximately represented.

In situ data

The present method requires meteorological observations of temperature and precipitation. In this article, near-surface air temperature and precipitation data from Kaza meteorological station (Figure 1) are used. The station is located at 3600 m asl and ~ 25 km from the boundary of the Chandra basin. The minimum and maximum temperature, and precipitation (rainfall and snow water equivalent (s.w.e.)) records from 1984 to 2009 available at this station are used. Kaza station is located in the orogenic interior, and 28% of the average annual precipitation falls during summer and 72% in winter (Figure 2).

The temperature lapse rates (TLRs) at 3 month intervals required for the method are taken from the Snow and Avalanche Study Establishment (SASE) observatory at Patseo (pers. commun.). The observations of TLR are from the Automatic Weather Station (AWS) located at SASE Patseo observatory at 3800 m asl and near the snout of Patsio glacier (~ 4900 m asl), Chandra–Bhaga river basin, in the orogenic interior of the Greater Himalaya. The surface snow density, another variable required for the method to model monthly changes in the snow-melt factor of TI model, is also from Patseo observatory. Though the Patseo observatory is located at a lower elevation, we use snow density observed at Patseo for higher elevation glaciers assuming similar rate of change of snow density with time at all elevations.

Mass-balance data for Chhota Shigri from 2002/03 to 2008/09 from the glaciological method are obtained from the literature^{36,37}. Mass-balance estimates from field measurements for Hamtah glacier from 2001 to 2008 are taken from unpublished reports of the Geological Survey of India (GSI).

Remote sensing data

To locate the position of snowlines in the ablation season, Landsat-5 Thematic Mapper (L5 TM), Landsat-7 Enhanced TM Plus (L7 ETM+) and Advanced Wide Field Sensor (AWiFS) remote-sensing data for 10 years (2000–2009) are used. A total of 59 satellite images (33 from Landsat and 26 from AWiFS) with least cloud cover are selected. Data for year 2003 are not used because of gap in the satellite imageries.

The Global Digital Elevation Model (GDEM) of Advanced Space-borne Thermal Emission and Reflection Radiometer (ASTER) is used in this study to delineate elevation contours on glaciers. The data have a 1 arc-sec horizontal resolution with a vertical accuracy of 17 m

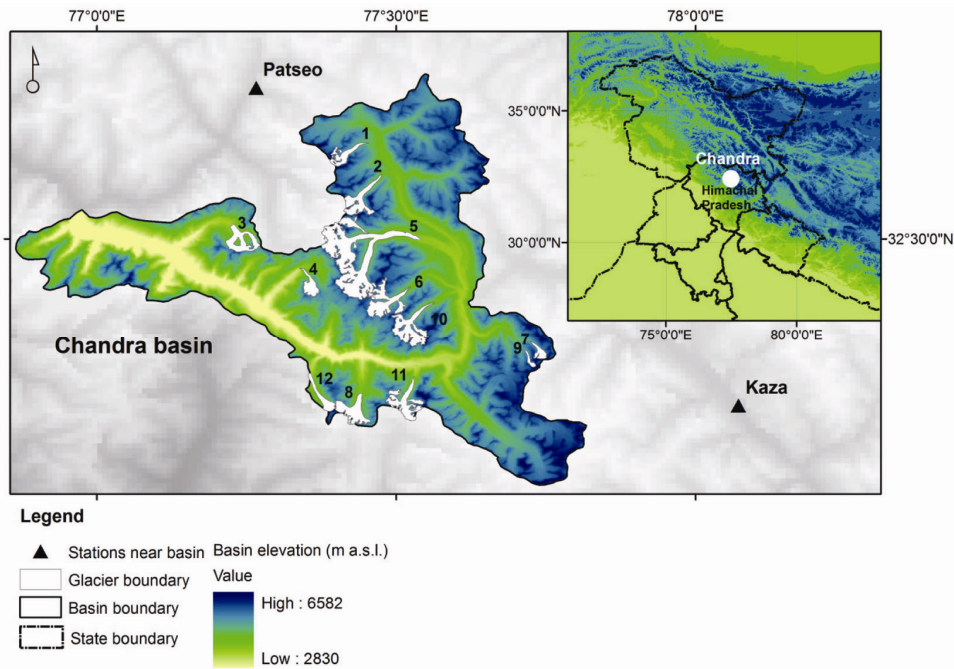


Figure 1. Map of the Chandra basin, Western Himalaya showing location of the selected individual glaciers (Table 1). The colour scale indicates elevation range (m asl). The locations of two *in situ* monitoring stations, Patseo (3800 m asl) and Kaza (3600 m asl) are marked by triangles. Temperature and precipitation records for the present study are taken from Kaza station, and data for temperature lapse rate and snow density are from Patseo station.

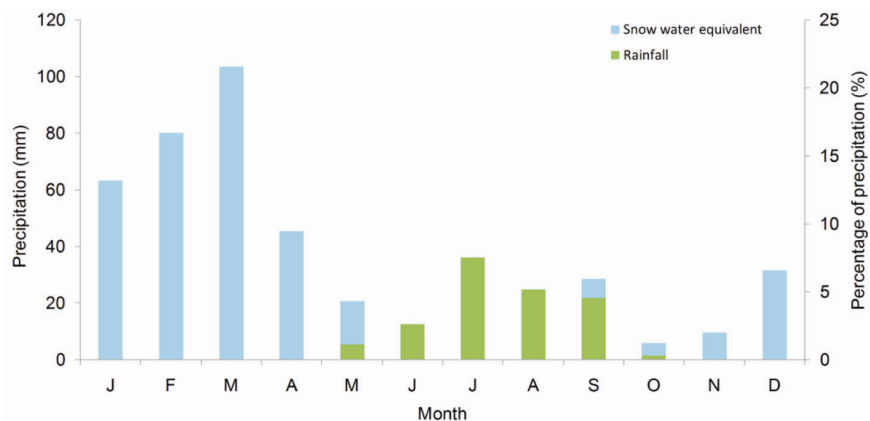


Figure 2. Climatological mean monthly precipitation at Kaza meteorological station from 1984 to 2009. The histogram shows both monthly precipitation and percentage contribution of monthly precipitation to the annual total precipitation. Blue colour indicates snowfall and green colour indicates rainfall. This station is situated in the orogenic interior of the Western Himalaya and receives the highest precipitation in winter months due to western disturbances: 28% of annual mean precipitation is received in summer and 72% in winter.

(11 m) on global scale (Himalayan terrain)³⁸. In addition, the glacier numbers, boundaries and attributes are adapted from Randolph Glacier Inventory version 4 (RGI v4)³⁹.

Methodology

The method involves estimation of: (i) transient snowlines on satellite images in the ablation season; (ii) total summer ablation (May–September) at each altitude; (iii) precipitation gradient in the vertical for the basin; (iv) post-

monsoon and winter accumulation (September–May) at each altitude; (v) model-derived ELA and AAR, and (vi) annual specific mass balance using a regression developed between mass balance and AAR (Figure 3 and Table 2).

Satellite-derived transient snowlines

The visible and infrared bands of Landsat TM and AWiFS are used to identify transient snowlines (TSL_{sat}). For determining the elevation of TSL, we rely on the

Table 1. Topographic characteristics of the 12 selected glaciers in the Chandra basin, Western Himalaya

Index	Glacier number	Area (km ²)	Minimum elevation (m asl)	Maximum elevation (m asl)	Slope (degree)	Aspect (degree)
1	20,668	8.95	4770	6195	20	135
2	20,689	14.74	4555	6425	15	90
3	20,715	13.91	4062	5752	26	0
4	20,726	7.42	3881	5594	27	225
5	20,739	77.87	4153	6069	14	135
6	20,770	26.56	4506	6047	16	90
7	20,986	5.16	5096	6064	16	0
8	21,094	14.12	4340	5924	18	180
9	21,887	2.14	5121	6096	19	0
10	20,313	22.70	4453	6169	15	0
11	21,083 (Chhota Shigri)	15.57	4240	6089	18	0
12	21,138 (Hamtah)	3.77	4036	4984	20	0

Glacier number, area, slope and aspect are taken from RGI v4 global glacier inventory and elevation information is taken from ASTER DEM.

hypsothetic curves of individual glaciers. The uncertainty in satellite-derived snowline elevation is estimated by adding independent sources of uncertainty^{27,40}: (i) altitude estimation by DEM (11 m); (ii) variations in slope near TSL and (iii) spatial variation of elevation along TSL.

Total ablation

Cumulative ablation during summer at elevation bands of 50 m interval is obtained using TI model. Ablation during October–April is assumed to be negligible because the temperature is mostly below freezing point. At a given altitude *j*, the cumulative amount of ablation *M_j* (mm) at the glacier surface on the *n*th day from 1 May is given by

$$M_j = \sum_{i=1}^n F_{\text{snow},i,j} \cdot \text{PDD}_{i,j}, \tag{1}$$

where *F_{snow}* is snow melt factor (mm °C⁻¹ d⁻¹) and PDD is positive degree-days (°C). The daily minimum and maximum temperature, and PDD are computed at each elevation using temperature data and TLR observations. The snowmelt factor is derived using the empirical relationship between snow density and melt factor⁴¹

$$F_{\text{snow}} = 11 \cdot (\rho_s / \rho_w), \tag{2}$$

where ρ_s and ρ_w are the density (kg m⁻³) of snow and water respectively. To account for the metamorphic transformation of snow, ρ_s at each altitude is increased when air temperature at that elevation is above freezing point (PDD > 0), i.e. melting begins at that elevation. The date in the ablation season when the melt starts at each elevation is recorded. The time interval between that date and 30 September is divided into five equal intervals, and ρ_s is increased in those intervals. This takes into account

spatial as well as temporal variations in snow density and hence melt factors. Our estimates of snow melt factor range between 2.31 and 3.85 mm °C⁻¹ day⁻¹, which is comparable with constant snow melt factor of 4 mm °C⁻¹ day⁻¹ used by Huss *et al.*³⁴.

Precipitation gradient and total accumulation

At the elevation of transient snowline, the amount of snow melt balances accumulation⁴². This definition is used to calculate total accumulation at TSL_{sat} and estimate the precipitation gradient between TSL_{sat} and the meteorological station. The cumulative melt from 1 May to TSL_{sat} day and altitude are calculated using the TI model. All TSL_{sat} used in this analysis are before the first summer snowfall on glacier, i.e. between 1 June and 30 September, so that winter accumulation remains uninterrupted by summer snowfall. The precipitation gradient *P_{grad}* (%m⁻¹) is then derived using the equation

$$P_{\text{grad}} = \frac{(P_{\text{TSL}} - P_{\text{STN}}) * 100}{(\Delta z * P_{\text{STN}})} = \frac{(\sum_{n=1}^D a_n - C_0) * 100}{(\Delta z * C_0)}, \tag{3}$$

where *P_{TSL}* and *P_{STN}* are precipitation accumulated at the elevation of TSL and meteorological station respectively. The elevation difference between TSL_{sat} and the meteorological station is Δz , *a_n* is the ablation (mm d⁻¹) at the level of TSL_{sat} on day and the summation in the term gives the cumulative ablation from 1 May up to TSL_{sat} day (*D*). The parameter *C₀* is post-monsoon and winter accumulation (mm) at the meteorological station.

The average precipitation gradient for the basin is calculated using snowlines on the 12 glaciers. This is then used to calculate total accumulation at each elevation. Accumulations by avalanches and wind drift are not taken into account.

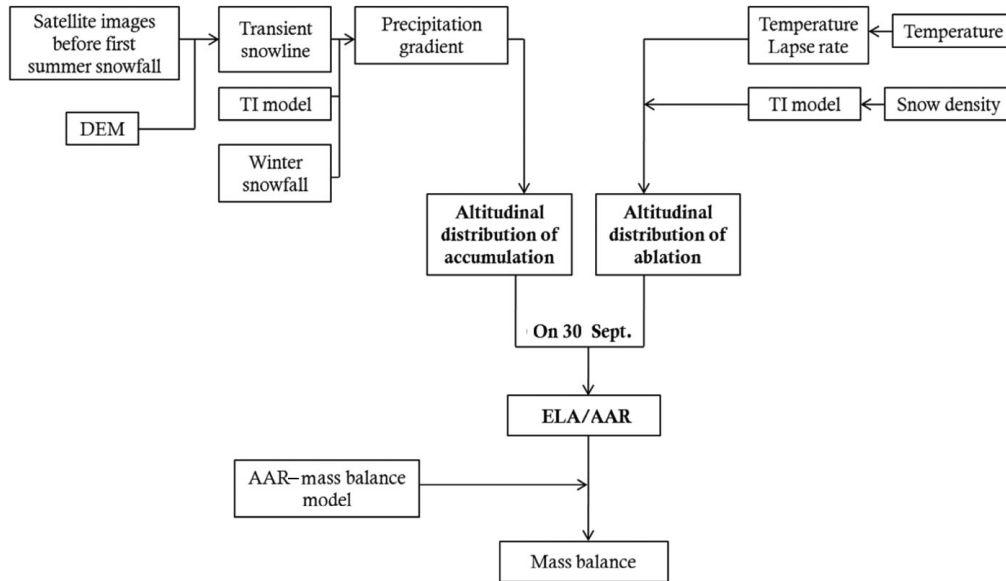


Figure 3. Flow chart representing the methodology adopted in the present study. It includes the following major procedures: calculation of (a) satellite-based transient snowlines; (b) altitudinal distribution of melt; (c) precipitation gradient; (d) altitudinal distribution of accumulation equilibrium line altitude; (e) ELA and area accumulation ratio (AAR), and (f) mass balance.

Table 2. Parameters used in the present study for the 12 selected glaciers

Parameter	Values
Elevation (m asl)	3875–6475
Lapse rate ($^{\circ}\text{C km}^{-1}$)	7.7 (MAM) 7.9 (JJA) 9.1 (SON)
Snow melt factor ($\text{mm } ^{\circ}\text{C}^{-1} \text{ day}^{-1}$)	2.31 2.37 3.08 3.63 3.85
Precipitation gradient ($\% \text{ km}^{-1}$)	190 ± 180

Modelled ELA, AAR and mass balance

The model altitudinal distribution of ablation and accumulation is used to monitor positions of TSL in summer months. The TSL calculated at the end of a glaciological year, i.e. 30 September is referred to as the modelled ELA (ELA_{mod}). The ELA_{mod} and hypsometry of glaciers are used to obtain the modelled AAR (AAR_{mod}). However, as discussed earlier, elevation of ELA_{mod} will be close but may not necessarily be the same as field-derived ELA, which could lead to errors in mass-balance estimates. In order to minimize this error, we have regressed modelled AAR with field mass balance for Chhota Shigri glacier. This regression relationship is then applied to other glaciers in the basin to calculate mass balance.

The general regression equation between AAR and mass balance is²³

$$B = a * \text{AAR} - b, \quad (4)$$

where B is the annual specific mass balance (cm water equivalent (w.e.)) of the glacier and AAR is accumulation area to the total glacier area ratio.

Uncertainty analysis

The uncertainty in modelled mass balance is estimated by adding uncertainty in (i) TSL estimation and (ii) AAR–mass balance relationship. Uncertainty in TSL estimates mainly arise from (i) station temperature (T); (ii) station snowfall (P); (iii) TLR (γ); (iv) precipitation gradient (P_{grad}), and (v) snow density (ρ). The uncertainty in modelled TSL is calculated using error propagation formula for multiple, repetitive and independent variables⁴³. The uncertainty in any quantity z which is a function of a set of independent variables is given as

$$\delta z = \sqrt{\left(\frac{\partial z}{\partial T} \delta T\right)^2 + \left(\frac{\partial z}{\partial P} \delta P\right)^2 + \left(\frac{\partial z}{\partial \gamma} \delta \gamma\right)^2 + \left(\frac{\partial z}{\partial P_{\text{grad}}} \delta P_{\text{grad}}\right)^2 + \left(\frac{\partial z}{\partial \rho} \delta \rho\right)^2}, \quad (5)$$

where δT , δP , $\delta \gamma$, δP_{grad} and $\delta \rho$ are the uncertainties in the measurements of the variables T , P , γ and P_{grad} and ρ

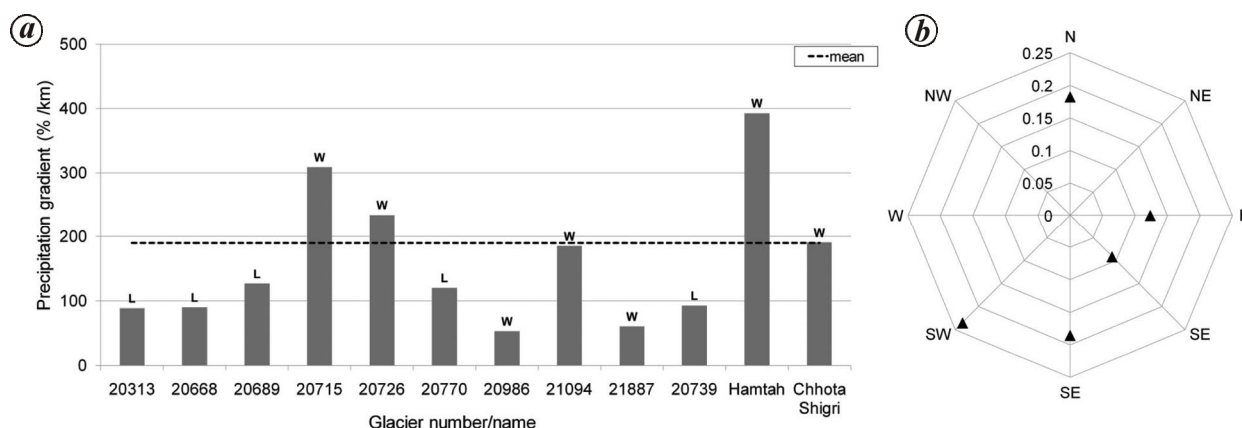


Figure 4. *a*, Estimated precipitation gradients (% km⁻¹; in the vertical direction) for the 12 selected glaciers in the Chandra basin. Dashed line represents the mean value of precipitation gradient used in this analysis. L (W) on the bars indicates whether the glacier is located on the leeward (windward) side of the westerly winds. *b*, Variation of precipitation gradient (% km⁻¹; along the radial axis) with orientation (azimuth). The gradients are averaged for glaciers with the same aspect. Glaciers in the southwest direction exhibit the highest precipitation gradient likely due to the influence of westerlies in the winter season.

respectively. Here, values for δT and δP are taken from standards of World Meteorological Organization (WMO) as 0.1°C and 2% respectively⁴⁴. We take standard deviation in our estimate of precipitation gradient for the basin as the uncertainty in P_{grad} . The uncertainty in $\delta\gamma$ is taken as 0.5°C/km. Further, we set $\delta\rho$ to be 30% of the mean measured snow density in ablation season which takes into account the change in melt factor by 1 mm °C⁻¹ d⁻¹. The calculated uncertainty in TSL is converted into uncertainty in AAR and mass balance by combining all hypsometric information of selected glaciers.

To estimate error due to the use of eq. (4) developed for the Chhota Shigri glacier on other glaciers with varying geomorphology, we compare mass-balance estimates using eq. (4) and field observations on Naradu glacier, Baspa basin. We chose Naradu glacier because Baspa basin is adjacent to Chandra basin. Field AAR of Naradu glacier for the years 2000/01–2002/03 (ref. 45) is used in eq. (4) to obtain modelled mass balance. The RMSE between field and model mass balance of Naradu glacier is used to assess the applicability of the regression developed in Chhota Shigri to neighbouring glaciers.

Results

Precipitation gradient over the Chandra basin

Potentially one could construct 708 glacier snowlines from the 59 satellite images on the 12 selected glaciers. However, since we consider only cloud-free days and days before first summer snowfall on the glacier, we are left with only 272 snowlines to calculate the mean precipitation gradient. We calculate the mean precipitation gradient for the 12 selected glaciers in the Chandra basin as $190 \pm 180\% \text{ km}^{-1}$ or $440 \pm 60 \text{ mm km}^{-1}$. The precipitation gradient ranges from 53 to 393% km⁻¹ (Figure 4a), with the mean at 70th percentile, indicating skewness in

the distribution. The large standard deviation in precipitation gradient is likely due to large variability in regional orography which controls spatial distribution and amount of precipitation^{28,46,47}.

The highest (lowest) precipitation gradient is calculated for glaciers oriented in southwest (east and southeast) direction (Figure 4b), possibly because the southwest-facing glaciers are situated on the windward side of the westerlies. A positive correlation of 0.65 is found between the slope and precipitation gradient of glaciers, suggesting that the glaciers in the Chandra basin with steep slopes and slopes exposed to western disturbances receive more precipitation during winter.

Our estimate of $190 \pm 180\% \text{ km}^{-1}$ for precipitation gradient is likely to result in reasonable estimates of accumulation on the glaciers in the Chandra basin, because the estimated accumulation in post-monsoon and winter season (September–May) on the Chhota Shigri glacier for 2001–2009, i.e. +1.17 m w.e.a⁻¹ is close to +0.94 m w.e.a⁻¹ (November–April for 2001–2012) reported by Azam *et al.*⁴⁸, though the precipitation gradient in their study (0.20 m km⁻¹) is smaller than the present analysis (0.44 m km⁻¹). This difference in the precipitation gradients may be due to topography and location of weather stations. The aforementioned study uses data from Bhuntar station (1039 m asl) situated at the orogenic front, which receives most of the annual precipitation in the monsoon season. However, we used data from Kaza station (3600 m asl) situated in the same valley of the Chandra basin, which predominantly receives precipitation from the westerlies.

Satellite-derived and modelled transient snowlines

Monthly averaged snowlines over 12 glaciers are estimated using satellite-derived transient snow lines

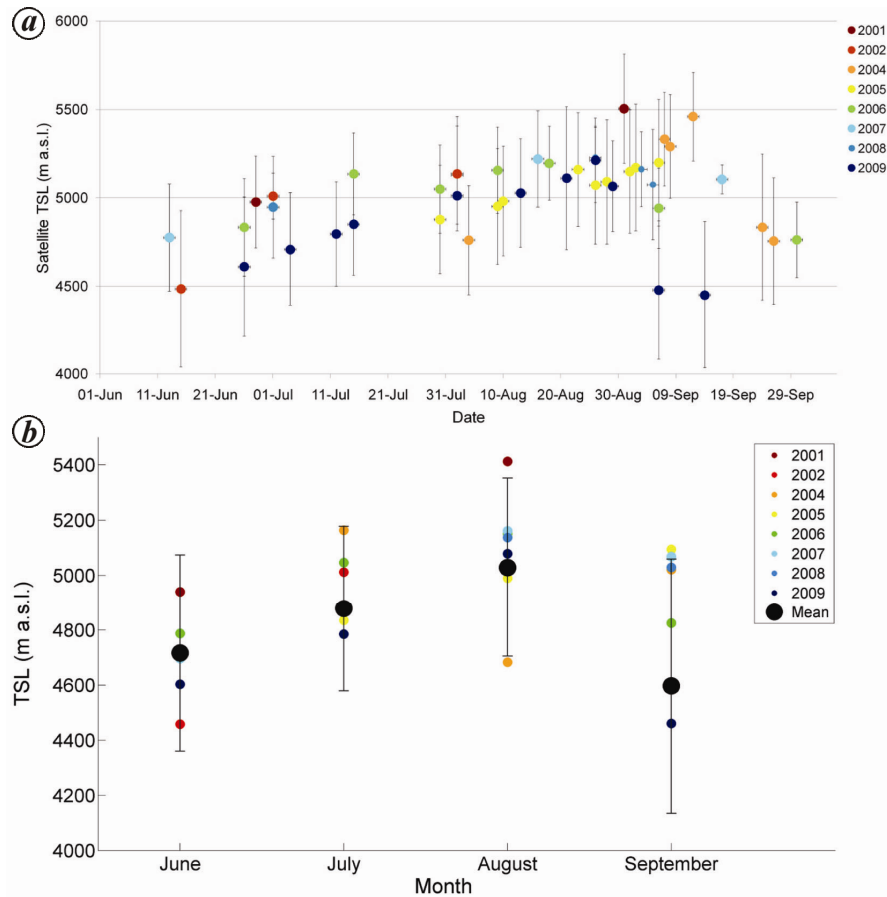


Figure 5. *a*, Elevation of satellite-derived transient snowlines and *b*, monthly averages in the ablation season from 2001 to 2009 averaged over the 12 selected glaciers (see Figure 1). The vertical bar in (*a*) indicates the standard deviation in snowline altitude which includes glacier-to-glacier variability, and in (*b*) it also includes the year-to-year variability. The colour dots represent positions of the snowline in different years. The mean for each month is shown by the large filled circle in (*b*).

(Figure 5). A total of 497 snowlines during the entire ablation period from 2001 to 2009 are used. The mean altitude of snowline increases progressively from 4716 ± 357 m asl in June to 5029 ± 324 m asl, i.e. maximum in August. Here, the uncertainty estimates are given by the standard deviation. In September, mean elevation of transient snowline declines by 432 m to 4597 ± 462 m asl. Variability in mean altitude of snowline from glacier to glacier is possibly due to topography and orientation of the glaciers⁴⁹. However, inter-annual variation is likely due to temperature and precipitation²⁷. Here, the uncertainty estimated in satellite-derived TSL altitude is ± 230 m.

The present analysis indicates that the satellite-derived highest average snowline of the study area occurs in August, which is considered as ELA in the conventional AAR method. However, the melt season extends to the end of September or early October, when the field measurements take place⁵⁰. The simulated fraction of monthly snowmelt with respect to the total melt in summer (May–September) increases progressively from May (6.25%) to August (33.53%), and also shows 17% of melt in

September. Therefore, the elevation of modelled snowlines increases throughout the ablation season and reaches a maximum in September (Figure 6), unlike satellite-derived snowlines (Figure 5). Hence, the decline in the elevation of TSL in September in satellite images (Figure 5) is likely erroneous, because of fresh snowfall.

The correlation between satellite-derived and modelled snowlines before the first summer snowfall on the glaciers is 0.58. The mean Δ TSL (satellite-derived TSL–modelled TSL) is calculated as 2.07 ± 433.96 m. Approximately 83% of all the Δ TSL values are within ± 500 m. The vertical movement of satellite-derived and modelled TSLs for four glaciers and for four different years, shown in Figure 6, indicates that overall the present model is in qualitative agreement with satellite-derived snowlines in the ablation season. The quantitative difference between modelled and satellite-derived TSLs is likely due to (i) use of mean precipitation gradient for all the glaciers; (ii) assumptions in the TI model that the snowmelt depends only on temperature and (iii) modelled TSL elevation represents one point on the glacier while satellite-derived TSL is spatially averaged elevation of TSL.

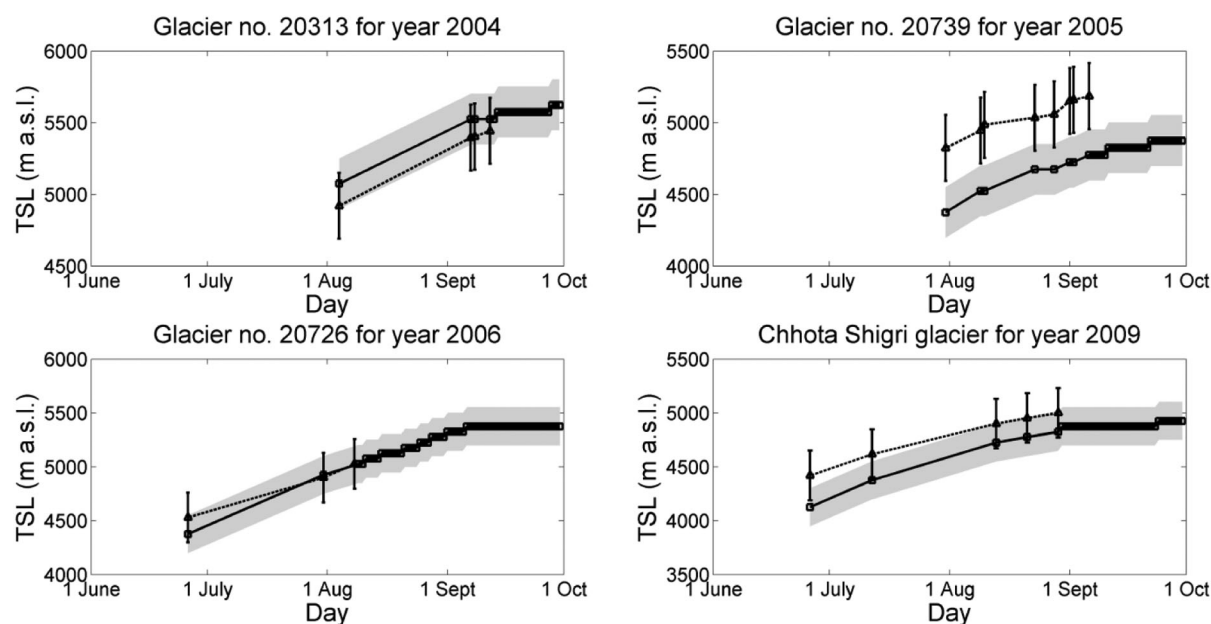


Figure 6. Vertical movement of satellite- and model-derived transient snowlines in the ablation season. The snowlines are shown only for glaciers (and years) where there are at least four satellite images in the ablation season. The solid lines with squares indicate the mean modelled snowlines in the ablation season and the shading represents uncertainty (± 210 m; see text). The dotted lines with triangles show the satellite-derived snowlines from the start of ablation season to the highest elevation in summer. Though there is some overestimation/underestimation in the altitude of the modelled snowlines, the model successfully captures the typical upward migration of observed snowlines in the ablation season.

New regression and mass balance of Chhota Shigri and Hamtah glaciers

Once we estimate ELA and AAR using the present method, we develop a regression fit between field mass balance and modelled AAR for Chhota Shigri glacier from 1987/88–88/89 to 2002/03–2008/09 (ref. 17). The regression relation is

$$B = 174.6 * AAR - 123.2, \quad (6)$$

where B is the annual specific mass balance (cm w.e.) of the glacier. We find a good correlation between field mass balance and modelled AAR, with r^2 of 0.83. According to eq. (6), the AAR representing zero mass balance is 0.7 whereas it is 0.5 in Kulkarni *et al.*²³. When compared with Kulkarni *et al.*²³, the slope of eq. (6) is reduced which implies more negative mass balance for the same AAR. A comparison of mass-balance estimates using eq. (6) and other regressions in the literature for the Western Himalaya is given in Table 3, which shows that the RMSE between field and modelled mass balance using eq. (6) for Chhota Shigri is the lowest. Equation (6) also converges to the regression developed for the Western Himalayan glaciers (Table 3), indicating that it can also be used for other glaciers in the Western Himalaya.

For comparing the modelled mass balance with conventional AAR method (Figure 7), we calculate the

annual specific mass balance using the highest satellite-derived snowline in the ablation season in eq. (4). The values for a and b for the conventional AAR method are adapted from Kulkarni *et al.*²³. The uncertainty in the conventional AAR method is estimated using uncertainty in satellite-derived TSL and AAR–mass-balance equation of Kulkarni *et al.*²³ for Naradu glacier. While the conventional method underestimates the mass loss, there is good agreement between modelled and field estimates of mass balance (Figure 7). The cumulative mass balance using the conventional AAR method is -0.24 ± 3.00 m w.e. for the period 2003/04–2008/09. This is an underestimate of mass loss when compared to field estimates of -4.27 ± 2.40 m w.e. for the same period. RMSE and correlation between field and conventional AAR method is 0.81 m w.e. and 0.68 respectively. For the same period, model-estimated mass balance is -4.68 ± 2.04 m w.e. and RMSE and correlation are 0.26 m w.e. and 0.94 respectively. Hence the present method improves mass-balance estimates by reducing the mean absolute error by 50.44% compared with conventional AAR technique.

Since satellite images and Kaza station data are available, we are also able to calculate mass loss for the same period of available geodetic studies for Chhota Shigri glacier (Table 4). For the period 1999/2000–2003/04, annual mass balance of Chhota Shigri glacier derived using geodetic method is -1.03 ± 0.44 m w.e.a⁻¹ (ref. 20). In agreement with the aforementioned study, the present method estimates mass loss of -1.16 ± 0.34 m w.e.a⁻¹ for

Table 3. Estimation of glacier cumulative mass balance for Chhota Shigri glacier for the period 2002/03–2008/09 using different regressions between mass balance and accumulation area ratio (AAR). Modelled AAR is used in all these regressions to estimate mass balance. RMSE is calculated between regression-predicted annual mass balance and glaciological mass balance measurements. The cumulative mass balance from glaciological measurements for this period is -5.66 m w.e.

Regression developed for	Reference	Regression relation (x is AAR and y is mass balance)	Cum. mass balance (m w.e.)	RMSE (m w.e.)
Western Himalaya	17	$y = 205.7*x - 121.8$	-5.14	0.26
Baspa Basin	23	$y = 243.0*x - 120.2$	-4.42	0.34
Chhota Shigri glacier	17, 36	$y = 381.3*x - 242.5$	-10.73	0.95
Chhota Shigri glacier	This present study	$y = 174.6*x - 123.2$	-5.76	0.25

Table 4. Comparison of mass balance using different methods for Chhota Shigri and Hamtah glaciers in the Chandra basin

Glacier	Study period	Present study (m w.e. a ⁻¹)	Conventional AAR method* (m w.e. a ⁻¹)	Glaciological method (m w.e. a ⁻¹)	Geodetic method (m w.e. a ⁻¹)
Chhota Shigri	1999–2004	-1.16 ± 0.34	-0.24 ± 0.50		-1.03 ± 0.44 (ref. 20)
	1999–2011	-0.93 ± 0.34	-0.06 ± 0.50		-0.39 ± 0.15 (refs 19, 20)
	2002–2008	-0.95 ± 0.34	-0.09 ± 0.50	-0.97 ± 0.40 (refs 36, 37)	-0.69 ± 0.43 (ref. 51)
Hamtah	2000–2002	-1.23 ± 0.34	-0.87 ± 0.50	-1.53^{**}	
	2003–2008				
	1999–2011	-1.23 ± 0.34	-0.79 ± 0.50		-0.45 ± 0.15 (ref. 20)

*Mass balance estimates by the conventional AAR method do not include the year 2003 due to satellite data gap.

**GSI unpublished reports. m.w.e.a⁻¹, Meter water equivalent per annum.

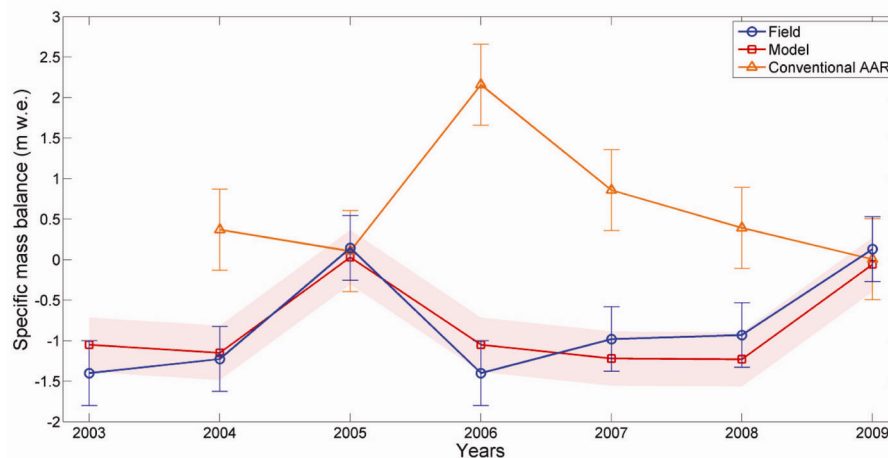


Figure 7. The annual specific mass balance (m w.e.) of Chhota Shigri glacier from 2002/03 to 2008/09 using field^{36,37} (blue), the present method (red) and conventional AAR method (orange). The shading around the red line represents the uncertainty in the modelled estimate (± 0.34 m w.e.; see text).

the same period (Table 4). However, mass balance of Chhota Shigri glacier from 1999/2000 to 2003/04 using the conventional AAR method is underestimated at -0.24 ± 0.50 m w.e.a⁻¹.

For the years 2002/03–2007/08, mass loss of approximately -0.69 ± 0.43 m w.e. a⁻¹ for Chhota Shigri glacier is available using elevation change over a $2^\circ \times 2^\circ$ cell around the glacier using ice, cloud and land elevation satellite (ICESat) altimetry data (Table 4)⁵¹. The modelled mass balance of -0.95 ± 0.34 m w.e.a⁻¹ for the same

period is comparable with the results of Käab *et al.*⁵¹ and glaciological mass balance (-0.97 ± 0.40 m w.e.a⁻¹). However, mass loss is underestimated by the conventional AAR method at -0.09 ± 0.50 m w.e.a⁻¹ for this period too. The annual mass loss estimated for the longer period of 1999/2000–2010/11 using geodetic approach²⁰ is smaller (-0.39 ± 0.15 m w.e.a⁻¹) than the modelled mass loss of Chhota Shigri calculated for the years 1999/2000–2008/09 (-0.93 ± 0.34 m w.e.a⁻¹). Even for this longer period, we find that the conventional AAR

Table 5. Comparison of modelled mass balance (in m w.e.) for the period 1999/2000–2008/09 with geodetic mass balance from Gardelle *et al.*¹⁹ for the period 1999/2000–2010/11 for eight glaciers in the Chandra basin

Glacier	Present study (m w.e. a ⁻¹)	Conventional AAR method (m w.e. a ⁻¹)	Geodetic method (m w.e. a ⁻¹)	Departure of model from geodetic (%)
Chhota Shigri	-0.93 ± 0.34	-0.06 ± 0.50	-0.39 ± 0.15	-138.46
Hamtah	-1.23 ± 0.34	-0.79 ± 0.50	-0.45 ± 0.15	-173.33
20689	-0.70 ± 0.34	-0.05 ± 0.50	-0.87	19.54
20313	-0.63 ± 0.34	+0.13 ± 0.50	-0.26	-142.31
20770	-0.72 ± 0.34	-0.07 ± 0.50	-0.49	-46.94
20739	-0.76 ± 0.34	-0.09 ± 0.50	-0.59	-28.81
21887	-0.34 ± 0.34	-0.13 ± 0.50	-0.50	32
20986	-0.39 ± 0.34	0.04 ± 0.50	-0.51	23.53
Mean	-0.71 ± 0.34	-0.13 ± 0.50	-0.51	-39.22

method underestimates the mass loss over Chhota Shigri glacier.

Mass balance for Hamtah glacier calculated for 2000/01–2001/02 and 2003/04–2007/08 using the present model is -1.23 ± 0.34 m w.e.a⁻¹, which agrees well with field-observed mass loss of -1.53 m w.e.a⁻¹ (Table 4). However, for the same period the conventional AAR method underestimates the mass loss at -0.87 ± 0.50 m w.e.a⁻¹. The field and modelled estimates of mass loss on Hamtah for the years 1999/2000–2008/09 are quite high compared to the geodetic mass balance value for years 1999/2000–2010/11 (ref. 20) (Table 4). The aforementioned study suggests that the discrepancy between geodetic approach and field estimates could be due to lack of field survey in accumulation zones of some glaciers in this region.

Mass balance of eight selected glaciers in Chandra basin

The model-derived mass balance is also compared with the available geodetic estimates of eight glaciers including Chhota Shigri and Hamtah in the Chandra basin (Table 5). The modelled mass balances (1999/2000–2008/09) differ on individual glaciers compared to geodetic mass balance (1999/2000–2010/11) using data of Gardelle *et al.*¹⁹. The departure of modelled mass balance from geodetic approach ranges from -173.33% to +32.00%. However, mean modelled mass loss (-0.71 ± 0.34 m w.e. a⁻¹) is comparable with geodetic estimates (-0.51 m w.e.), indicating that it may converge at a larger scale as suggested by Vincent *et al.*²⁰. However, in all the cases, the conventional AAR method (1999/2000–2001/02, 2003/04–2008/09) highly underestimates the mass loss.

The reason for discrepancy between modelled and geodetic mass balance estimates on individual glaciers (Table 5) could be: (i) elevation biases on small glaciers and data gaps due to presence of clouds and shadows in the geodetic data²⁰; (ii) glacier-to-glacier variations in

seasonal mass balance corrections⁵²; (iii) geodetic approach includes basal and internal mass changes of the glaciers on longtime scale⁵², whereas modelled mass budgets are restricted to the surface, and (iv) variations in incoming solar radiation received due to different aspects of glaciers are ignored in the present model.

Application of the method on basin level

To demonstrate that the present approach can be applied on a basin scale, the annual specific mass balance for the 12 selected glaciers is simulated for the decade of 1999/2000–2008/09 (Table 1; Figure 8a and b). We find that the highest positive annual mass balance is obtained for 2004/05, when there was comparatively heavy winter precipitation and low temperature in the ablation season (Figure 8a). The largest negative annual mass balance was in the year 2000/01, when it was warmer and winter precipitation was smaller. Almost all the analysed glaciers were losing mass during 1999/2000–2008/09 (Figure 8b). The largest negative cumulative mass balance of 0.59 ± 0.26 Gt is simulated for Samudratapu glacier (glacier no. 20739), while nearly stable mass balance of $+0.007 \pm 0.007$ Gt is estimated for glacier no. 21887 (Figure 8b). The 12 glaciers in the Chandra basin experience a mean mass loss rate of 0.79 ± 0.34 m w.e.a⁻¹. This translates to a total volume loss of 1.67 ± 0.72 Gt for the same period. Our results agree with recent studies^{53,54} that found a similar mass loss and retreat of glaciers in the Chandra basin.

Uncertainty estimates

The calculated change in snowline elevation with precipitation at Kaza station ($\partial Z/\partial P$) is -64 m per 10 mm increase in total winter precipitation, and the change in snowline elevation with temperature ($\partial Z/\partial T$) is calculated as $+107$ m per 1°C rise in temperature. Similarly, partial derivatives of ELA with respect to precipitation gradient, temperature lapse rate and snow density are calculated.

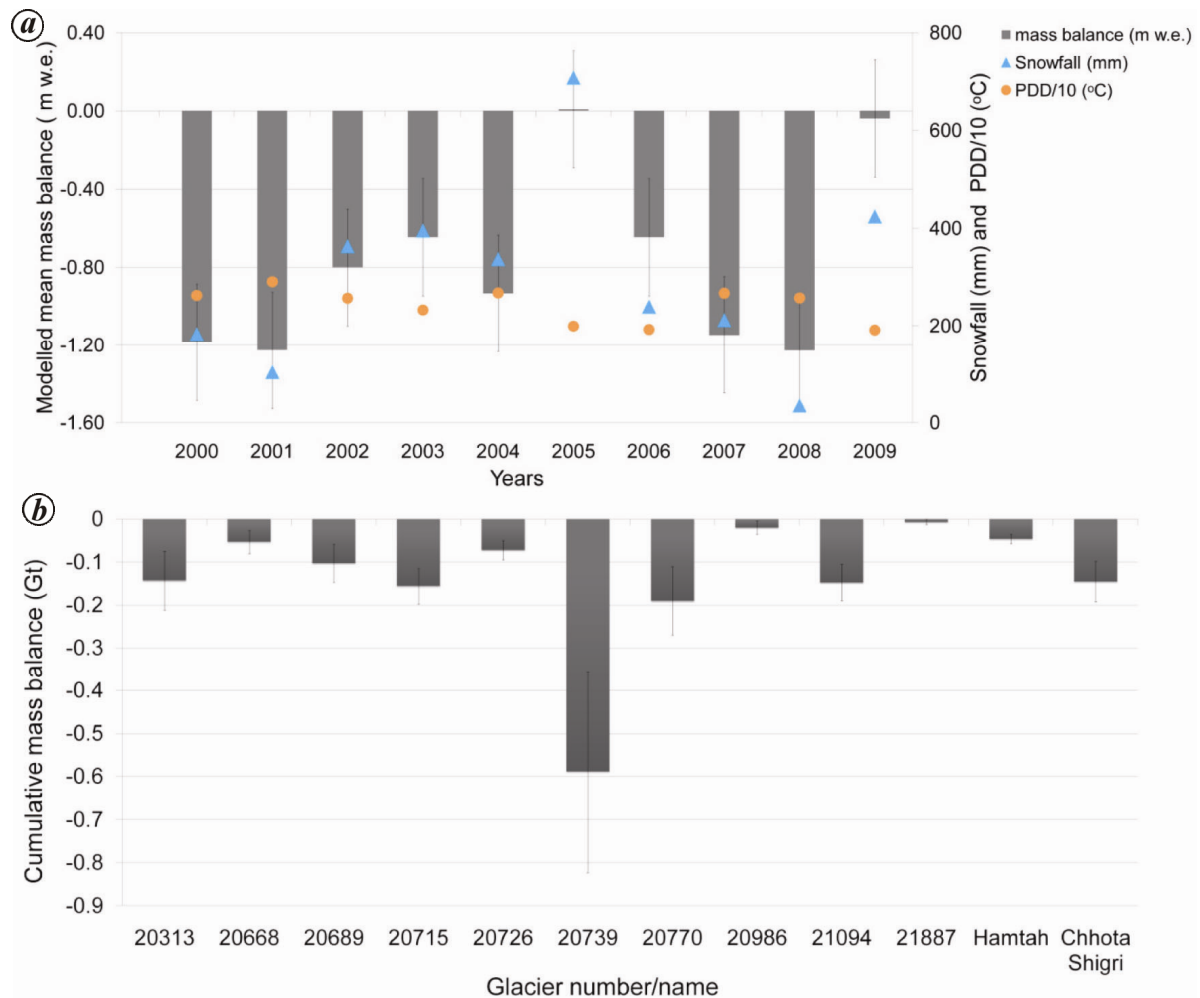


Figure 8. *a*, The modelled mean annual mass loss averaged over the 12 selected glaciers (Table 1) in the Chandra basin (bars). The blue colour triangles indicate total accumulation (September–May) at Kaza station in snow water equivalent (mm). The positive degree days (PDD) in the ablation season (May–Sept) at Kaza are indicated by orange-coloured dots. *b*, The modelled cumulative mass loss for selected glaciers in the Chandra basin from 1999/2000 to 2008/09. We can see that all the 12 selected glaciers are losing mass.

The change in snowline altitude with snow density ($\partial Z/\partial \rho$) is calculated as +81 m for a 30% change in snow density, which accounts for 1 mm °C⁻¹ day⁻¹ change in melt factor. Uncertainty in ELA is found to be less sensitive to changes in snow melt factor, which is also observed by Huss *et al.*³⁴. The elevation of snowline changes by -77 m for a 0.5°C km⁻¹ increase in lapse rate ($\partial Z/\partial \gamma$) and by -178 m for a 0.18% m⁻¹ increase in precipitation gradient ($\partial Z/\partial P_{\text{grad}}$).

Substituting all these values in eq. (5), we estimate that the uncertainty in the modelled snowline is ± 210 m. This uncertainty in ELA translates to an uncertainty in AAR of ± 0.19 . When it is used in eq. (6), we calculate an uncertainty of ± 0.34 m w.e. for model-derived annual specific mass balance. The uncertainty due to the use of eq. (6) developed on Chhota Shigri glacier to Naradu glacier is found as 0.01 m w.e., which adds negligible uncertainty to the total uncertainty in model mass balance.

Discussion and conclusion

Identification of ELA on satellite images is challenging; therefore in practice, the highest available satellite-derived transient snowline in the ablation season is considered as ELA in the conventional AAR method. However, this assumption usually leads to underestimation of mass loss. Therefore, we have developed a method that combines satellite images, a snowmelt model and meteorological measurements to locate the position of ELA. From the modelled ELA, modelled annual AAR is calculated and regressed against the field estimates of mass balance on Chhota Shigri glacier in the Chandra basin. This regression relationship is then used on several selected glaciers in the same basin to calculate mass balance. One advantage of our method is that the annual mass balance estimates are feasible even for years without satellite images as long as station meteorological data are available for that year.

We compare our modelled mass balance with field observations, the conventional AAR method and available geodetic estimates for the Chandra basin. We find that the conventional AAR method substantially underestimates the mass loss compared to field measurements on Chhota Shigri and Hamtah glaciers. Application of our method reduces the mean absolute bias in mass balance by 50.44% compared to the conventional AAR technique for Chhota Shigri glacier (Table 4). We also apply our method to six other glaciers where geodetic estimates are available (Table 5). The mean annual mass loss of $-0.71 \pm 0.34 \text{ m w.e.a}^{-1}$ for 1999/2000–2008/09 using the present method is comparable to the geodetic estimate of $-0.51 \text{ m w.e.a}^{-1}$ when averaged over all the eight selected glaciers. However, modelled mass loss differs from geodetic estimates on individual glaciers for longer time-period. For all the eight glaciers, the conventional AAR method underestimates mass loss, i.e. $-0.13 \pm 0.50 \text{ m w.e.a}^{-1}$. For some glaciers, the conventional method indicates mass gain whereas other approaches show mass loss.

As discussed earlier, the present method can be applied on basin scale. For the 12 selected glaciers in the Chandra basin, the analysis shows that cumulative loss is $1.67 \pm 0.72 \text{ Gt}$ ($-0.79 \pm 0.34 \text{ m w.e. a}^{-1}$) for the years 1999/2000–2008/09. Application of the method to all glaciers in the basin and estimation of mass balance of the entire basin will be the focus of our next study.

There are several limitations to the method proposed here. First, application of the approach needs *in situ* meteorological data from at least one station in or near the basin. Second, lack of field observation in a basin could limit validation of the method in that basin. The third limitation is that the method assumes the spatial distribution of snow depth within elevation zones is constant. However, in reality world snow depth could have spatial variations because of differences in snowfall and shadowing over rugged terrain. This could introduce some uncertainty in mass-balance estimates. Fourth, calculation of melt using TI model ignores the changes in incoming solar radiation due to different aspects and slopes of glaciers. However, this limitation can be avoided by including finer topographic features of the glaciers. Fifth, the situations where ELA crosses the highest elevation of glacier or mass balance changes with no shifts in the former, constrain the application of AAR–mass-balance relationship. Another limitation is that the method cannot be applied on glaciers extensively fed by avalanches, i.e. Turkestan-style glaciers. Further, the present method is applicable to alpine glaciers having distinct accumulation and ablation seasons.

The model-derived mass balance estimates clearly indicate that the 12 selected glaciers in the Chandra basin show retreat in the last decade. This could be because of the on-going climate change. There are indications that the current mass loss of glaciers could accelerate in the future^{9,11}. Since the present approach can be implemented

on a basin or regional scale when meteorological data are available, it can be used to infer the future deviations in mass balance when climate change projections of temperature and precipitation are incorporated into the method while keeping non-climatic variables constant.

1. Bolch, T. *et al.*, The state and fate of Himalayan glaciers. *Science*, 2012, **336**, 310–314.
2. Immerzeel, W. W., van Beek, L. P. H. and Bierkens, M. F. P., Climate change will affect the Asian water towers. *Science*, 2010, **328**, 1382–1385.
3. Kaser, G., Großhauser, M. and Marzeion, B., Contribution potential of glaciers to water availability in different climate regimes. *Proc. Natl. Acad. Sci. USA*, 2010, **107**(47), 20223–20227.
4. Fujita, K., Kadota, T., Rana, B., Kayastha, R. B. and Ageta, Y., Shrinkage of glacier AX010 in Shorong region, Nepal Himalayas in the 1990s. *Bull. Glacier Res.*, 2001, **18**, 51–54.
5. Ageta, K. Y., Naito, N., Iwata, S. and Yabuki, H., Glacier distribution in the Himalayas and glacier shrinkage from 1963 to 1993 in the Bhutan Himalayas. *Bull. Glacier Res.*, 2003, **20**, 29–40.
6. Nie, Y., Zhang, Y., Liu, L. and Zhang, J., Glacial change in the vicinity of Mt. Qomolangma (Everest), central high Himalayas since 1976. *J. Geogr. Sci.*, 2010, **20**(5), 667–686.
7. Bhabri, R., Bolch, T., Chaujar, R. K. and Kulshreshtha, S. C., Glacier changes in the Garhwal Himalaya, India, from 1968 to 2006 based on remote sensing. *J. Glaciol.*, 2011, **57**(203), 543–556.
8. Kamp, U., Byrne, M. and Bolch, T., Glacier fluctuations between 1975 and 2008 in the Greater Himalaya Range of Zaskar, southern Ladakh. *J. Mt. Sci.*, 2011, **8**(3), 374–389.
9. Chaturvedi, R. K., Kulkarni, A., Karyakarte, Y., Joshi, J. and Bala, G., Glacial mass balance changes in the Karakoram and Himalaya based on CMIP5 multi-model climate projections. *Climate Change*, 2014, **123**(2), 315–328.
10. Kulkarni, A. V. and Karyakarte, Y., Observed changes in Himalayan glaciers. *Curr. Sci.*, 2014, **106**(2), 237–244.
11. Shea, J. M., Immerzeel, W. W., Wagnon, P., Vincent, C. and Bajracharya, S., Modelling glacier change in the Everest region, Nepal Himalaya. *Cryosphere*, 2015, **9**(3), 1105–1128.
12. Xu, J., Grumbine, R. E., Shrestha, A., Eriksson, M., Yang, X., Wang, Y. and Wilkes, A., The melting Himalayas: cascading effects of climate change on water, biodiversity and livelihoods. *Conserv. Biol.*, 2009, **23**(3), 520–530.
13. Huss, M., Farinotti, D., Bauder, A. and Funk, M., Modelling runoff from highly glacierized alpine drainage basins in a changing climate. *Hydrol. Process.*, 2008, **22**, 3888–3902.
14. Thayyen, R. J. and Gergan, J. T., Role of glaciers in watershed hydrology: a preliminary study of a ‘Himalayan catchment’. *Cryosphere*, 2010, **4**, 115–128.
15. Paterson, W. S. B., *Physics of Glaciers*, Portsmouth, Butterworth-Heinemann, NH, USA, 3rd edn, 2000.
16. Engelhardt, M., Schuler, T. V. and Andreassen, L. M., Contribution of snow and glacier melt to discharge for highly glacierised catchments in Norway. *Hydrol. Earth Syst. Sci.*, 2014, **18**(2), 511–523.
17. Pratap, B., Dobhal, D. P., Bhabri, R., Mehta, M. and Tewari, V. C., Four decades of glacier mass balance observations in the Indian Himalaya. *Reg. Environ. Change*, 2016, **16**, 643–653.
18. Berthier, E., Arnaud, Y., Kumar, R., Ahmad, S., Wagnon, P. and Chevallier, P., Remote sensing estimates of glacier mass balances in the Himachal Pradesh (Western Himalaya, India). *Remote Sensing Environ.*, 2007, **108**(3), 327–338.
19. Gardelle, J., Berthier, E., Arnaud, Y. and Kääb, A., Region-wide glacier mass balances over the Pamir–Karakoram–Himalaya during 1999–2011. *Cryosphere*, 2013, **7**(4), 1263–1286.
20. Vincent, C. *et al.*, Balanced conditions or slight mass gain of glaciers in the Lahaul and Spiti region (northern India, Himalaya)

- during the nineties preceded recent mass loss. *Cryosphere*, 2013, 7(2), 569–582.
21. Tshering, P. and Fujita, K., First *in situ* of decadal glacier mass balance (2003–2014) from the Bhutan Himalaya. *Ann. Glaciol.*, 2016, 57(71), 289–294.
 22. Kulkarni, A. V., Mass balance of Himalayan glaciers using AAR and ELA methods. *J. Glaciol.*, 1992, 38(128), 101–104.
 23. Kulkarni, A. V., Rathore, B. P. and Alex, S., Monitoring of glacial mass balance in the Baspa basin using accumulation area ratio method. *Curr. Sci.*, 2004, 86(1), 185–190.
 24. Kaser, G., Fountain, A. and Jansson, P., A manual for monitoring the mass balance of mountain glaciers, IHP–VI. Technical Documents in Hydrology, UNESCO, Paris, 2003.
 25. Cogley, J. G. *et al.*, Glossary of glacier mass balance and related terms, IHP–VII. Technical Documents in Hydrology, No. 86, IACS Contribution No. 2, UNESCO-IHP, Paris, 2011.
 26. Bamber, J. L. and Rivera, A., A review of remote sensing methods for glacier mass balance determination. *Global Planet. Change*, 2007, 59(1–4), 138–148.
 27. Rabatel, A. *et al.*, Can the snowline be used as an indicator of the equilibrium line and mass balance for glaciers in the outer tropics? *J. Glaciol.*, 2012, 58(212), 1027–1036.
 28. Arora, M., Singh, P., Goel, N. K. and Singh, R. D., Spatial distribution and seasonal variability of rainfall in a mountainous basin in the Himalayan region. *Water Resour. Manage.*, 2006, 20(4), 489–508.
 29. Brahmabhatt, R. M., Bahuguna, I., Rathore, B. P., Kulkarni, A. V., Shah, R. D. and Nainwal, H. C., Variation of snowline and mass balance of glaciers of Warwan and Bhut basins of western Himalaya using remote sensing technique. *J. Indian Soc. Remote Sensing*, 2011, 40(4), 629–637.
 30. Mir, R. A., Jain, S. K., Saraf, A. K. and Goswami, A., Detection of changes in glacier mass balance using satellite and meteorological data in Tirunghkad basin located in western Himalaya. *J. Indian Soc. Remote Sensing*, 2013, 42(1), 91–105.
 31. Rai, P. K., Nathawat, M. S. and Mohan, K., Glacier retreat in Doda Valley, Zaskar Basin, Jammu & Kashmir, India. *Universal J. Geosci.*, 2013, 1(3), 139–149.
 32. Kulkarni, A. V., Effect of climatic variations on Himalayan glaciers: a case study of upper Chandra River basin, Himachal Pradesh. In *Remote Sensing Applications*, Paper presented at the Indo-US Symposium–Workshop on Remote Sensing and its Application, Mumbai, 1996.
 33. Rabatel, A., Dedieu, J. P. and Vincent, C., Using remote-sensing data to determine equilibrium-line altitude and mass-balance time series: validation on three French glaciers, 1994–2002. *J. Glaciol.*, 2005, 51(175), 539–546.
 34. Huss, M., Sold, L., Hoelzle, M., Stokvis, M., Salzmann, N., Farinotti, D. and Zemp, M., Towards remote monitoring of sub-glacier mass balance. *Ann. Glaciol.*, 2013, 54(63), 85–93.
 35. Sangewar, C. V. and Shukla, S. P., *Inventory of the Himalayan Glaciers: A Contribution to the International Hydrological Programme*, Geological Survey of India, Special Publication No. 34, 2009, p. 169.
 36. Wagnon, P. *et al.*, Four years of mass balance on Chhota Shigri Glacier, Himachal Pradesh, India, a new benchmark glacier in the western Himalaya. *J. Glaciol.*, 2007, 53(183), 603–611.
 37. Azam, M. F. *et al.*, From balance to imbalance: a shift in the dynamic behaviour of Chhota Shigri glacier, western Himalaya, India. *J. Glaciol.*, 2012, 58(208), 315–324.
 38. Fujita, K., Suzuki, R., Nuimura, T. and Sakai, A., Performance of ASTER and SRTM DEMs, and their potential for assessing glacial lakes in the Lunana region, Bhutan Himalaya. *J. Glaciol.*, 2008, 54(185), 220–228.
 39. Pfeffer, W. T. *et al.*, The Randolph Glacier Inventory: a globally complete inventory of glaciers. *J. Glaciol.*, 2014, 60(221), 537–552.
 40. Yuwei, W. U., Jianqiao, H. E., Zhongming, G. and Anan, C., Limitations in identifying the equilibrium-line altitude from the optical remote-sensing derived snowline in the Tien Shan, China. *J. Glaciol.*, 2014, 60(224), 1117–1125.
 41. Martinec, J., Sonwmelt-runoff model for stream flow forecast. *Nordic Hydrol.*, 1975, 6(3), 145–154.
 42. Ostrem, G., ERTS data in glaciology – an effort to monitor glacier mass balance from satellite imagery. *J. Glaciol.*, 1975, 15(73), 403–415.
 43. Taylor, J. R., *An Introduction to Error Analysis: the Study of Uncertainties in Physical Measurements*, University Science Books, Sausalito, California, 2nd edn, 1982.
 44. World Meteorological Organization, *Guide to Meteorological Instruments and Methods of Observation*, WMO, Switzerland, 2008, 7th edn.
 45. Koul, M. N. and Ganjoo, R. K., Impact of inter- and intra-annual variation in weather parameters on mass balance and equilibrium line altitude of Naradu Glacier (Himachal Pradesh), NW Himalaya, India. *Climate Change*, 2010, 99(1–2), 119–139.
 46. Bookhagen, B. and Burbank, D. W., Topography, relief, and TRMM-derived rainfall variations along the Himalaya. *Geophys. Res. Lett.*, 2006, 33(8), 1–5.
 47. Tawde, S. A. and Singh, C., Investigation of orographic features influencing spatial distribution of rainfall over the Western Ghats of India using satellite data. *Int. J. Climatol.*, 2015, 35(9), 2280–2293.
 48. Azam, M. F., Wagnon, P., Patrick, C., Ramanathan, A. L., Linda, A. and Singh, V. B., Reconstruction of the annual mass balance of Chhota Shigri glacier, Western Himalaya, India, since 1969. *Ann. Glaciol.*, 2014, 55(66), 69–80.
 49. Pandey, P., Kulkarni, A. V. and Venkataraman, G., Remote sensing study of snowline altitude at the end of melting season, Chandra-Bhaga basin, Himachal Pradesh, 1980–2007. *Geocarto Int.*, 2013, 28(4), 311–322.
 50. Azam, M. F., Wagnon, P., Vincent, C., Ramanathan, A. L., Favier, V., Mandal, A. and Pottakkal, J. G., Processes governing the mass balance of Chhota Shigri glacier (western Himalaya, India) assessed by point-scale surface energy balance measurements. *Cryosphere*, 2014, 8, 2195–2217.
 51. Käab, A., Berthier, E., Nuth, C., Gardelle, J. and Arnaud, Y., Contrasting patterns of early twenty-first-century glacier mass change in the Himalayas. *Nature*, 2012, 488, 495–498.
 52. Fischer, A., Comparison of direct and geodetic mass balances on a multi-annual timescale. *Cryosphere*, 2011, 5(1), 107–124.
 53. Pandey, P. and Venkataraman, G., Changes in the glaciers of Chandra–Bhaga basin, Himachal Himalaya, India, between 1980 and 2010 measured using remote sensing. *Int. J. Remote Sensing*, 2013, 34(15), 5584–5597.
 54. Mandal, A., Ramanathan, A. and Angchuk, T., Assessment of lahoul-spiti (western Himalaya, India) glaciers – an overview of mass balance and climate. *J. Earth Sci. Climatic Change*, 2014, S11:003.
- ACKNOWLEDGEMENTS. We thank the Divecha Centre for Climate Change, Indian Institute of Science, Bengaluru for providing laboratory facilities. ASTER GDEM is a product of METI and NASA. We also thank the US Geological Survey for providing free on-line data products such as Landsat level 1 products and ASTER GDEM for research purposes; Etienne Berthier, LEGOS, The National Center for Scientific Research (CNRS), France for sharing geodetic estimates for the Chandra basin; Dr H. S. Negi (Snow & Avalanche Study Establishment, DRDO, Chandigarh) for valuable suggestions; and the Space Applications Centre (SAC) and Bhakra Beas Management Board for AWiFs data and *in situ* meteorological data respectively.

Received 6 July 2016; accepted 2 September 2016

doi: 10.18520/cs/v111/i12/1977-1989